Ocean Sci., 2, 249–266, 2006
www.ocean-sci.net/2/249/2006/
© Author(s) 2006. This work is licensed
under a Creative Commons License.

Ocean Science

Mechanisms controlling primary and new production in a global ecosystem model – Part I: Validation of the biological simulation

E. E. Popova, A. C. Coward, G. A. Nurser, B. de Cuevas, M. J. R. Fasham, and T. R. Anderson

National Oceanographic Centre, Southampton, UK

Received: 12 June 2006 – Published in Ocean Sci. Discuss.: 31 July 2006
Revised: 26 October 2006 – Accepted: 21 November 2006 – Published: 6 December 2006

Abstract. A global general circulation model coupled to a simple six-compartment ecosystem model is used to study the extent to which global variability in primary and export production can be realistically predicted on the basis of advanced parameterizations of upper mixed layer physics, without recourse to introducing extra complexity in model biology. The "K profile parameterization" (KPP) scheme employed, combined with 6-hourly external forcing, is able to capture short-term periodic and episodic events such as diurnal cycling and storm-induced deepening. The model realistically reproduces various features of global ecosystem dynamics that have been problematic in previous global modelling studies, using a single generic parameter set. The realistic simulation of deep convection in the North Atlantic, and lack of it in the North Pacific and Southern Oceans, leads to good predictions of chlorophyll and primary production in these contrasting areas. Realistic levels of primary production are predicted in the oligotrophic gyres due to high frequency external forcing of the upper mixed layer (accompanying paper Popova et al., 2006) and novel parameterizations of zooplankton excretion. Good agreement is shown between model and observations at various JGOFS time series sites: BATS, KERFIX, Papa and HOT. One exception is the northern North Atlantic where lower grazing rates are needed, perhaps related to the dominance of mesozooplankton there. The model is therefore not globally robust in the sense that additional parameterizations are needed to realistically simulate ecosystem dynamics in the North Atlantic. Nevertheless, the work emphasises the need to pay particular attention to the parameterization of mixed layer physics in global ocean ecosystem modelling as a prerequisite to increasing the complexity of ecosystem models.

Correspondence to: E. E. Popova
(ekp@noc.soton.ac.uk)

1 Introduction

The global ocean can be viewed as an organised system of physically driven, biologically controlled chemical cycles, which influence planetary climate over large spatial and temporal scales (Ducklow, 2003). This paradigm has led to sustained interest in the range of contrasting ecosystem structures, and their consequences for export of carbon to the ocean interior. Interest in regional time-series studies (multiple volumes of the Deep-Sea Research, Part II) gave rise to the development of one-dimensional ecosystem models with parameters fitted to reproduce the local observations (e.g. Bissett et al., 1999; Pondaven et al., 2000; Hood et al., 2001; Anderson and Pondaven, 2003). The realistic representation of biophysical interactions in global modelling studies poses an even greater challenge to the modelling community. These studies ideally require a single generic parameter set that is capable of capturing ecosystem dynamics throughout the world ocean. Parameters can no longer be tuned to suit individual locations without regard for consequences elsewhere in the model. Such a parameter set is by no means easy to obtain. For example, (Fasham, 1995) was unable to model the contrasting ecosystem dynamics in the North Atlantic and North Pacific oceans without having to resort to alternate parameters for each site.

Simple ecosystem models – nutrient-phytoplankton-zooplankton-detritus (NPZD) – have provided the basis of global biogeochemical modelling studies (e.g. Six and Maier-Reimer, 1996; Bopp et al., 2001; Palmer and Totterdell, 2001). It has been widely emphasised that the next step in global modelling should be an increase in the sophistication of the ecosystem models used for this purpose (Doney, 1999), building on the lessons learned from the one-dimensional modelling studies. Possible advances include the incorporation of multi-nutrient limitation, size structure, plankton geochemical and functional groups, the microbial loop and cycling of dissolved organic matter, and improved

Published by Copernicus GmbH on behalf of the European Geosciences Union.

representations of subsurface particle transport and remineralisation. Following this route, Moore et al. (2002) developed a global ecosystem model that includes multielement limitation of phytoplankton growth (Fe, N, P, Si) and several algal groups, run on a simplified global mixed layer grid. The model was able to reproduce patterns observed in field data from nine diverse oceanic localities.

Despite the current emphasis on increasing complexity of ecosystem models in General Circulation Models (GCMs), it is important not to forget to pay attention to model physics. Put succinctly, "biogeochemical models are only as good as the physical circulation framework in which they are set" (Doney, 1999). In spite of the recent realisation that mesoscale physics plays an important role in the control of new production (e.g., McGillicuddy Jr. et al., 1998), physical model improvement does not simply mean increasing the resolution of the model grid as much as possible. It also requires that vertical mixing, and in particular dynamics of the upper mixed layer (UML), are realistically represented in models. Stratification of the water column affects not only light limitation of primary productivity and nutrient supply, but other aspects of ecosystem dynamics as well. For example, the depth of the winter UML may influence the ability of different types of zooplankton to overwinter. (Banse, 1996) in his review of the factors controlling all year round low Chl-a in the Southern Ocean argued that the overwintering stock of microzooplankton was important in subsequent grazing control of the spring bloom.

Mixed layer schemes used in 3-D global biogeochemical modelling studies are often simplistic, despite the major influence of the UML dynamics on the marine ecosystem and biogeochemical cycling. They tend not to capture short-term variability in the UML, which is important in ecosystem dynamics. The use of very simplistic formulations and lack of temporal resolution are both significant. For example, the model of (Aumont et al., 2003) has a 100 m photic zone that is representative of the UML depth, with convective events producing mixing of the neighbouring 50 m vertical grid cells. The use of long time steps is a common feature of global models subjected to long integrations. For example, the model of (Six and Maier-Reimer, 1996) uses a time step of one month. Similarly the bulk Krauss-Turner mixed layer scheme employed by (Palmer and Totterdell, 2001) uses monthly mean external forcing as well as suffering from homogenising concentrations throughout even the deepest UMLs. The most advanced treatment of UML dynamics in 3-D global biogeochemical GCMs is in the modelling study of Bopp et al. (2001), which uses a 1.5 order turbulent closure scheme (Blanke and Delecluse, 1993). This model does nevertheless suffer difficulties, such as being unable to predict realistic winter mixed layers in the North Pacific and Southern Ocean, showing excessive deep convection in both areas.

In this paper we investigate the extent to which the combination of an advanced representation of water column stratification in a global 3-D GCM (Ocean Circulation and Climate Advanced Modelling project, OCCAM) coupled to a simple (NAPZD) ecosystem model is able to effectively predict global primary and export production. An accompanying paper (Popova et al., 2006) hereafter abbreviated to PC06, investigates the role of short-term variability of the ocean mixing in plankton productivity and presents a detailed sensitivity analysis of model results to the frequency of external forcing. The emphasis of our work is thus on providing a high-level representation of processes associated with UML physics rather than increasing the complexity of the ecosystem model. The role of temporal and geographical variability of the UML depth in ecosystem dynamics are examined. Results are presented both for the global ocean, and also in detail for various JGOFS (Join Global Ocean Flux Study) time series stations.

2 Description of the coupled model

2.1 Physical model

OCCAM is a z-level global ocean model originating from the works of Bryan (1969), Semtner (1974), Cox (1984) and the Modular Ocean Model (MOM) (Pacanowski, 1995). The model solves the ocean primitive equations on a horizontal staggered "B" grid (Arakawa, 1966). The most important extra features of OCCAM include a free surface, the use of a split-QUICK scheme for the horizontal advection of tracers (Webb, 1998), an iso-neutral mixing scheme (Griffies, 1998), a two-grid system to avoid a singularity at the North Pole (Coward et al., 1994), a vertical mixing scheme (see below) and a complex sea ice model (Aksenov, 2002).

Different configurations of OCCAM have horizontal resolutions of 1, $\frac{1}{4}$, $\frac{1}{8}$ and $\frac{1}{12}^{\circ}$ in both meridional and zonal directions. All three resolutions employ the same vertical spacing with 66 levels varying in thickness from 5 m in the top surface 50 m to 200 m at depth. The biological model discussed here is coupled with the 1° physical model. At this resolution we also employ a Gent and McWilliams eddy flux parameterization (Griffies, 1998). OCCAM uses the "K profile parameterization" (KPP) vertical mixing scheme (Large et al., 1997) with certain adjustments described in Appendix A. KPP was developed for use in global ocean models. It includes a scheme for determining boundary layer depth, where the turbulent contribution to the vertical shear of a bulk Richardson number is parameterized. The diffusivity throughout the boundary layer is formulated to agree with similarity theory of turbulence in the surface layer and is subject to the conditions that both it and its vertical gradient match the interior values at the bottom of the boundary layer. The most significant difference between the KPP scheme and bulk models is that the UML does not need to be well mixed. Compared to second- moment models, KPP produces a more realistic exchange of properties between the mixed layer and

the thermocline. In particular, models such as those developed by Gaspar et al. (1990) and Mellor and Yamada (1974) tend to underestimate this exchange (Large et al., 1997).

Another feature of KPP that is especially important for biological applications is the ability to handle successfully not only the annual cycle of the UML but also events of the order of only a day in duration. The KPP model has been shown to simulate many such events very well, including convective boundary layer deepening, diurnal cycling, storm induced deepening (Large et al., 1997) and short-term spring shoaling of the UML layer (see discussion below).

Our ocean model is forced by air-sea fluxes of momentum, heat and freshwater. Input fields of wind speed, air temperature, specific humidity, sea level pressure, cloudiness, precipitation and short wave radiation are used, together with the model top level potential temperature, to compute the heat and freshwater forcing to be applied at each (hourly) time step. The input data for the period 1985–2002 have been supplied by NCAR and are described in (Large et al., 1997). The six-hourly zonal and meridional 10 m wind components, surface 2 m air temperature and specific humidity are from the NCEP reanalysis (Kalnay et al., 1996). Cloud fraction data are based on the ISCCP C1 dataset (Rossow and Schiffer, 1991). The solar radiation and precipitation are based on the daily ISCCP (Bishop and Rossow, 1991) and monthly microwave Sounding Unit (MSU) (Spencer, 1993) satellite data products, respectively. The Bishop and Rossouw data covers the period 1984–1991, after which the solar radiation field is filled in with climatology. We have further imposed a diurnal cycle upon the incoming shortwave flux by taking into account the angle of the sun above the horizon at each timestep and location. This is done in such a way as to ensure the net daily amount is maintained. Where available, the (Xie and Arkin, 1997) observational precipitation data has been blended with the MSU climatology. The code to calculate the surface forcing has been adapted from the NCAR CSM Ocean Model (NCAR/TN-423+STR). Due to the large uncertainties in the freshwater fluxes, a restoring term is included which is derived from the difference between the model sea surface salinities and the monthly climatological values from the (Levitus and Boyer, 1994) and (Levitus et al., 1994) climatology. The relaxation coefficent is chosen to provide the equivalent of a 30 day timescale for relaxing the top 20m.

2.2 Biological model

The biological model state variables are phytoplankton (P), zooplankton (Z), detritus (D), nitrate (N), ammonium (A) and chlorophyll-a (Chl). A detailed description of the biological sources and sinks is given in Appendix B. The model is based on the approach of (Fasham et al., 1990) and (Fasham and Evans, 1995), although without a representation of bacteria and dissolved organic matter. The further differences from the (Fasham et al., 1990) model are alternative parameterizations of zooplankton excretion, and incorporation of Chl into the model as an additional state variable.

Zooplankton excretion is a biomass-specific term in most ecosystem models (e.g. Fasham et al., 1990). Instead here we make this excretion a fraction of ingestion. 70% of assimilated food is allocated to production, with the remaining 30% being excreted directly as ammonium. The basic assumption is that metabolic rate (and associated excretion) is proportional to growth rate, which is a reasonable assumption in the case of small zooplankton (Fenchel and Finlay, 1983). The single zooplankton compartment in the model represents all zooplankton types in the ocean, but in particular the microzooplankton which dominate grazing in many areas.

The Chl model state variable was added to assist model validation. The largest source of available data for phytoplankton biomass is satellite-measured Chl-a concentration. The Chl:C ratio in phytoplankton is however highly variable, ranging from $\sim$0.003 to $>$0.1 mg Chl mgC^{-1} (Cloern and Grenz, 1995) and so the assumption of a fixed ratio in global models impairs the validation against Chl data. The Equation for Chl employed here is based on the model of (Taylor et al., 1997) with a fixed phytoplankton $C{:}N$ ratio (see Appendix B).

2.3 Control run

The physical model was spun up for 8 years. This consisted of a 4 year "robust diagnostic" integration (relaxation of tracer values towards climatological values at all depths with a 1 year timescale of relaxation) followed by a repeated 4 year period with only surface forcing.

The biological model was coupled to the physics at the end of this procedure, corresponding to the beginning of 1989. The model was then integrated, in fully coupled mode with the evolving physical fields, over a 6-year period. The first three years were considered as a settling period and the subsequent four years (1992–1994, inclusive) were used for the analysis described below. For clarity and to help distinguish this model experiment from future configurations we shall refer to this run of the OCCAM 1° OGCM with Biology as OB1. Since no significant consistent trend in the nitrate field was detected in the upper ocean over the period of this run, we consider the integration time adequate for the purpose of this study. The initial nitrate distribution was derived from (Conkright et al., 2001) and the rest of the ecosystem state variables were set to 0.1 Mmol Nm^{-3}.

3 Results

3.1 UML variability

UML depth variability is a key factor in determining the geographical differences in the ecosystem dynamics in the ocean (Sverdrup, 1953; Longhurst, 1995). Although there are a

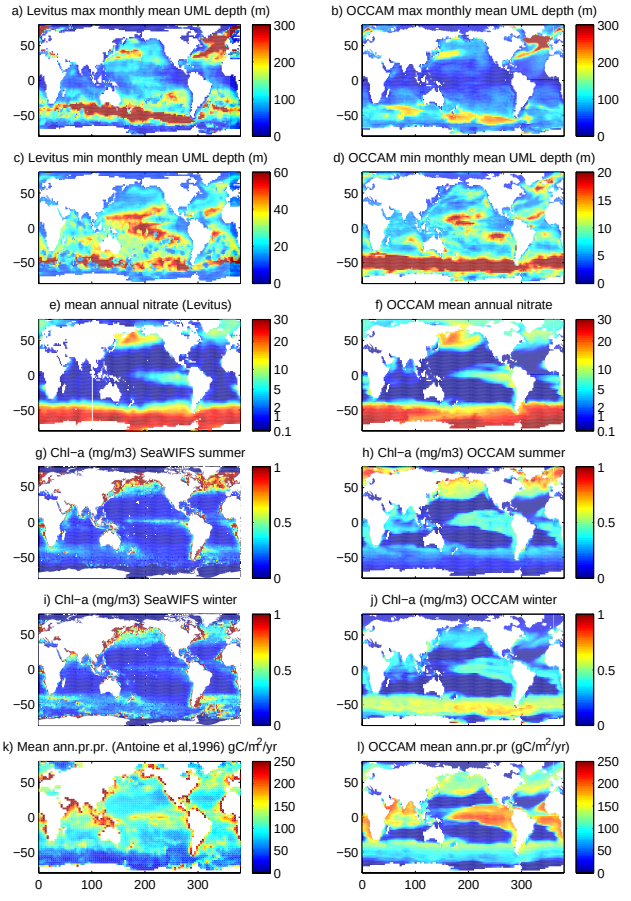

Fig. 1. (a)–(d) – maximum and minimum monthly mean UML depth (m) from the NMLD climatology (a), (c) and from the OB1 control run (b), (d), note changes in colour scale between OB1 and climatology; **(e)–(h)** – summer (April–September) and winter (October–March) Chl-a concentrations (mgChl m^{-3}) derived from the SeaWIFS (e), (g) and the OB1 control run (f), (h); **(i), (j)** – mean annual primary production (g C m^{-2} yr^{-1}) from Antoine et al. (1996) model based on CZCS ocean colour data (i) and from The OB1 control run (j); mean annual nitrate concentrations (mmol N m^{-3}) from the Conkright et al. (2001) climatology **(k)** and from the OB1 control run **(l)**.

significant number of observations for specific areas of the ocean (e.g. station Papa, discussed later), observational data on the global spatial and temporal UML depth variability are available only as monthly mean values derived from temperature (T) and salinity (S) climatologies. For the model UML depth verification we used maximum and minimum of the monthly UML depth (Fig. 1a, c) from the Naval Research Laboratory ocean mixing layer depth climatologies (NMLD) (http://www7320.nrlssc.navy.mil/nmld/nmld.html). Depths were calculated using a density-based criterion with a fixed-temperature difference of 0.8°C that was shown to be an optimal definition for the global domain (Kara et al., 2003). OB1 maximum and minimum monthly UML depth fields are shown in Fig. 1b, d. Minimum monthly UML depth was chosen for our analysis as a convenient proxy for the summertime average UML depth, and therefore the influence of light limitation on the primary production during the growing season. The maximum monthly UML depth was chosen as a proxy for the depth of the winter convective mixing, the main mechanism supplying nutrients to the surface layer, as well as the extent to which zooplankton can survive through the winter and hence exert grazing pressure on the spring phytoplankton bloom.

In general, qualitative agreement between OB1 UML and NMLD is excellent (Figs. 1a, c and 1b, d). Direct quantitative comparison of the modelled UML and NMLD should not be attempted for a number of reasons. First of all, UML depth definitions used in the climatology and in the OB1 are different, the first being density-based and the second buoyancy-based. Secondly, NMLD is calculated using 10 m depth as a reference, thus not allowing values less than 10 m and filtering out periods of short-term strong near-surface stratification. As will be shown later, even during winter convection such periods are quite frequent in OB1's UML variability and cause a bias toward shallower monthly mean values. Third, some areas such as the Southern Ocean have inadequate data coverage and any T and S observations are generally biased towards good weather conditions.

The most pronounced characteristic of both the OB1 UML and NMLD maximum monthly mean UML depths is areas of deep mixing at high latitudes, with maximum values in the North Atlantic occurring in the region of deep water formation poleward of 40° N in the Labrador sea, and Irminger and Iceland basins. The wintertime UML in the subpolar North Pacific does not deepen as much as in the Atlantic because of a barrier layer formed by a halocline that is maintained by precipitation and slow upwelling from below (Kara et al., 2000a,b). Similarly, very deep winter convection is not observed in the Southern Ocean, where stable water columns can occur despite sharp temperature inversions due to the compensating effect of salinity (Gloersen and Campbell, 1998). Except for the areas of deep water formation in the North Atlantic, the deepest winter UMLs, in both OB1 and NMLD, are found in the strong western boundary current regions of the Kuroshio and Gulf Stream, and in the Antarctic Circumpolar Current (ACC). Areas where maximum monthly mixing does not penetrate below 50 m are concentrated around the equator, spreading to about 20° S and 20° N.

The most pronounced feature of the minimum annual OB1 UML and NMLD is the extreme depth in the vicinity of the ACC between 40 and 60° S, almost twice as deep as anywhere else in the world ocean due to the high wind stress and high frequency of storm events. Relatively deep layers are also found on the equatorward peripheries of the subtropical gyres both in OB1 and NMLD, being especially pronounced in the Southern Pacific.

3.2 Global annual mean primary and new production

Estimates of the global primary production based on ^{14}C incubation data vary widely between 20 and 45 GtCyr^{-1} with one estimate of 60 to 80 GtCyr^{-1} (Sundquist, 1985; Berger et al., 1987). Estimates of global primary production based on sea-surface Chl-a concentrations derived from satellite data are 35–60 GtCyr^{-1} (Antoine et al., 1996; Gregg et al., 2003). The OB1 global primary production value of 38 GtCyr^{-1} is similar to these estimates and slightly lower than those arising from the 3-D global biogeochemical models of Six and Maier-Reimer (1996), Palmer and Totterdell (2001), Aumont et al. (2003) (43.6, 47.7, and 42.6 GtCyr^{-1}, respectively).

Global new production in OB1, based on the uptake of nitrate in the photic zone, is 8.5 Gt Cyr^{-1} (f-ratio equal to 0.22). It is difficult to verify this value on the basis of the observations. Estimates of new production (assuming steady state) on global or even basin scales are difficult to obtain. The most commonly used direct measure of new production is the uptake of nitrate estimated using ^{15} N tracer techniques. These measurements are local and restricted to short time periods. Other approaches include estimates of oxygen utilisation below the photic zone or nitrate supply to the photic zone and also are restricted to localised areas. Global export production, exactly equal to the global new production in our model, can also be used for verification of OB1 new production. However such estimates are available only from other modelling studies. Thus global export production estimates based on SeaWiFS-derived primary production using the model of (Behrenfeld and Falkowski, 1997), and applying various export production algorithms, vary between 11.1 and 20.9 GtCyr^{-1} (Laws et al., 2000). Global biogeochemical model estimates include 11.1 Gt Cyr^{-1} (Six and Maier-Reimer, 1996), 9.4 Gt Cyr^{-1} (Palmer and Totterdell, 2001), 10.6 Gt Cyr^{-1} (Aumont et al., 2003) and 11.1–13.1 Gt Cyr^{-1} (Bopp et al., 2001). The estimate of global new/export production in OB1 is in good agreement with both the satellite-derived and GCM modelling estimates. However both these approaches include large uncertainties and are difficult to constrain. Oschlies (2001) presented an excellent review of potential problems associated with the GCM estimates of new production. Such estimates are dependent on model architecture and the resultant amount of diapycnal mixing. Potential problems with satellite-derived export production are associated with the fact that it is based on the export models applied to the results of primary production algorithms, which in turn have large uncertainties (Campbell et al., 2002).

3.3 Global distributions of the Chlorophyll-a, primary production and nitrate

Satellite-based integrated primary production remains an important property for the validation of global biogeochemical models in spite of the significant uncertainties involved in its calculation (Campbell et al., 2002). It should be kept in mind that there are large differences between primary production estimates derived using the various existing algorithms. Nevertheless, a comparison of twelve algorithms in geographically diverse areas of the ocean found that the estimates of those that performed best were usually within a factor of two of ^{14}C estimates (Campbell et al., 2002). Mean summer (April–September) and winter (October–March) modelled and satellite-derived surface Chl distributions are compared in Fig. 1g–j. Figure 1k, l shows the simulated annual mean primary production as well as a satellite-derived estimate based on the model of Antoine et al. (1996). Finally, mean annual fields of nitrate from Conkright et al. (2001) and the OB1 run are shown in Fig. 1c, d. Because of the coarse horizontal resolution, OB1 does not adequately represent shelf areas with their enhanced Chl-a and primary production. These areas are omitted from the discussion below.

The most striking feature in the distributions of all three characteristics, both in the model and observations, is the existence of vast oligotrophic areas situated in the subtropical gyres with low nutrients, Chl-a and primary production. There are four major mechanisms of vertical transport of nutrients into the photic zone of the gyres: breaking of internal waves, mesoscale eddies, wind-driven Ekman pumping, and atmospheric storms. Seasonal changes in the UML in these regions are small compared with the rest of the ocean, and short-term UML deepening as a result of episodic storms is of major importance to the ecosystem in the gyres in general (PC06). The position of these domains is well reproduced by OB1 in the Southern hemisphere, although they are smaller than observed in the Northern Pacific and Atlantic Oceans and not very distinct in the North Indian Ocean. We can speculate that these discrepancies are because the poleward boundaries of oligotrophic gyres are constrained by the intensity of the lateral advection and diffusion of nutrients from the boundary currents towards the centre of the gyres. North Pacific and Atlantic currents in the Northern hemisphere and Antarctic Circumpolar Current in the Southern hemisphere (Longhurst, 1995) are much broader when simulated in a 1° model because of the insufficient horizontal resolution. This feature results in a broader distribution of nutrients in the 3-D model. The same applies to the equatorial currents, which determine the extent of the oligotrophic conditions towards the equator.

The underestimation of primary production in the oligotrophic gyres by an order (or even two orders) of magnitude is a perennial difficulty in global and basin-scale models (e.g. Sarmiento et al., 1993; Oschlies et al., 2000). This issue is related only in part to the ongoing debate on how to explain the factor of two discrepancy between geochemical estimates of new production in oligotrophic waters and vertical estimates of nutrient supply (e.g. Jenkins, 1982; McGillicuddy Jr. et al., 1998). We speculate that characteristic underestimation of primary production on the peripheries of the oligotrophic gyres in 3-D modelling studies is first of all associated with

the use of low frequency external forcing (e.g. monthly mean in Palmer and Totterdell, 2001, and Oschlies and Garçon, 1999). In these areas winter mixing can reach significant depths, and primary production is limited by nutrient availability only in summer. Light limitation plays the dominant role in winter, although primary production during this season remains high. Two mechanisms related to the short-term variability in the atmospheric forcing increase productivity in these areas (PC06). The first involves the existence of short-term periods of shallow stratification during calm weather in winter. During such periods, which last from one to two days, limitation by light is ameliorated and significant production occurs. The second mechanism involves storm-induced mixing in summer, which increases nutrient supply and therefore tends to increase productivity. in order to reproduce these mechanisms adequately, a resolution of at least 6 h is required for the external forcing fields (PC06).

A possible reason for extremely low predicted primary production in the central part of the oligotrophic areas of 3-D modelling studies may be the linear parameterization of zooplankton loss terms (excretion, mortality), typically leading to unrealistically low values of zooplankton biomass in oligotrophic regimes and hence low nutrient remineralisation. These problems are not experienced in OB1 in areas of subtropical gyres due to zooplankton excretion being parameterized in proportion to ingestion rather than biomass. Our estimates of primary production (30–50 $\mathrm{gC\,m^{-2}\,yr^{-1}}$) are only a factor of two or so lower than values presented in Antoine et al. (1996) based on CZCS-derived primary production (70–100 $\mathrm{gC\,m^{-2}\,yr^{-1}}$). Some of this difference may be explained by the fact that the model does not contain nitrogen fixation nor eddy-induced horizontal and vertical supply of nutrients, nor variable C:N ratio (e.g. Anderson and Pondaven, 2003). In addition, the satellite-derived estimates are also subject to error. Predicted Chl-a shows a strong subsurface maximum in the subtropical gyres which does not constitute a biomass or productivity maximum, but resulted mainly from an increase in the Chl-a to carbon ratio in phytoplankton. This maximum provided a relatively small contribution to total integrated productivity, a feature which is supported by Atlantic Meridional Transect observations (Maranon et al., 2000).

SeaWiFS summer and winter Chl-a fields, as well as satellite-derived primary production and observed nutrients, show enhanced values in a wide band around the equator (10° S–10° N). This enhancement is usually attributed to the influence of the equatorial upwelling (Williams and Follows, 2003). Our results indicate that this band consists of two areas, characterised by different physical regimes, but leading to similar ecosystem responses. One is the equatorial upwelling area with a shallow stable UML, surrounded by a second area of equatorial currents with a deeper UML than in the oligotrophic gyres. The latter area therefore has greater potential for light limitation, although the stronger storm-induced vertical mixing supplies nutrients into the photic zone thus enhancing primary production. OB1 shows equatorial increases in the Chl-a, primary production and nitrate similar to those observed, except that the enhanced equatorial band is latitudinally wider. This discrepancy is because the modelled equatorial currents are too broad and thus produce overestimated lateral fluxes of nutrients.

The highest values of primary production (about 200 $\mathrm{g\,C\,m^{-2}\,yr^{-1}}$) in OB1 are on the edges of the oligotrophic gyres, similar to the satellite-derived estimates of (Antoine et al., 1996). These high values are however in contradiction to the global primary production map of (Falkowski et al., 2003) which shows the maximum primary production in the Northern North Atlantic in a band between 45 and 65° N. The models of (Palmer and Totterdell, 2001) and (Oschlies et al., 2000) both show results similar to OB1, with predicted primary production reaching its maximum around 45° N and then decreasing towards higher latitudes. The OB1 Chl-a maximum does not correspond to the productivity maximum, being strictly in line with the area of deep convection where the effect of grazing on the spring bloom is minimal because of the inability of microzooplankton to maintain significant biomass under the condition of deep mixing. The highly productive edges of the oligotrophic gyres show only moderate annual Chl-a values of about 0.4–0.5 $\mathrm{mg\,Chl\,m^{-3}}$ because of the strong grazing control by microzooplankton, which can survive in the model through the winter if monthly mean UML depth does not reach values deeper than 150–200 m.

The most striking feature of the North Pacific ocean, both in OB1 and in SeaWiFS, is an absence of the high Chl-a values observed in the deep water formation area of the North Atlantic. Lack of deep winter convection in the North Pacific, with maximum UML depth reaching only 150–200 m (Fig. 1b), allows zooplankton in the model to survive efficiently through the winter and to suppress the spring phytoplankton bloom. Although primary production estimates in both OB1 and Antoine et al. (1996) are as high as in the North Atlantic, and nitrate concentrations are about two times higher than in the North Atlantic (10–20 $\mathrm{mmol\,N\,m^{-3}}$), the predicted mean annual Chl-a does not reach values higher than 0.5 $\mathrm{mg\,Chl\,m^{-3}}$.

The OB1 Southern Ocean primary production is relatively low (100–150 $\mathrm{g\,C\,m^{-2}\,yr^{-1}}$) due to strong light limitation. It is somewhat higher than the Antoine et al. (1996) satellite-derived estimates, but in good agreement with the most recent estimates of Arrigo et al. (1998) for the Indian sector of the Southern Ocean. Predicted Chl-a values are low all year around at about 0.4 $\mathrm{mg\,Chl\,m^{-3}}$ throughout most of the Southern Ocean.

3.4 Annual cycle of ecosystem characteristics at JGOFS time-series stations

Unless otherwise stated, observations of nutrients, UML depth, Chl-a, and primary production used in this section

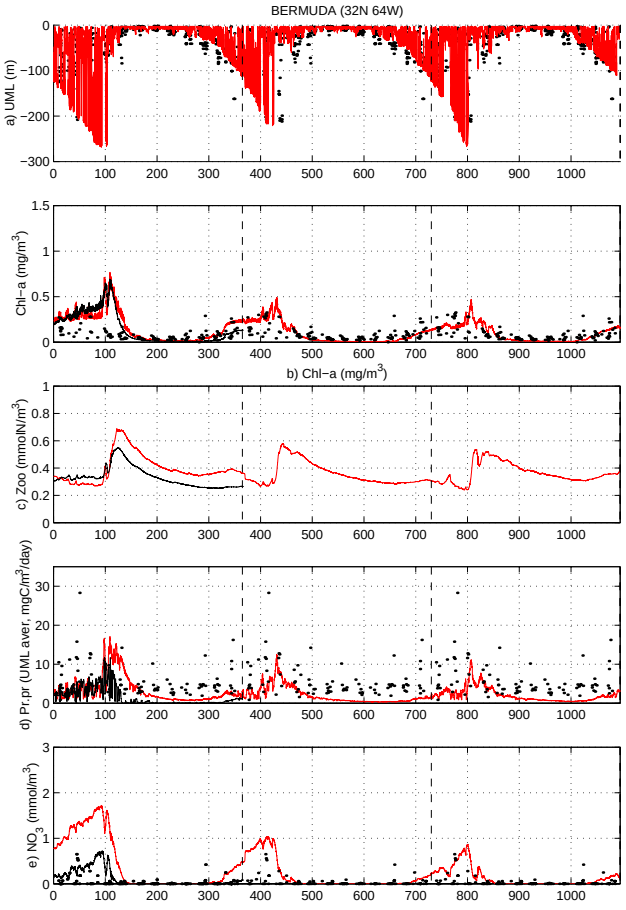

Fig. 2. Annual cycle of modelled (solid line) and observed (dots) ecosystem characteristics at BATS: **(a)** – UML depth (m), **(b)** – surface Chl-a (mg Chl m^{-3}), **(c)** – surface zooplankton biomass (mmol N m^{-3}), **(d)** – UML averaged primary production (mg C m^{-3} d^{-1}), **(e)** – surface nitrate concentration (mmol N m^{-3}). Results of the grazing experiment are shown for the first year as a black line.

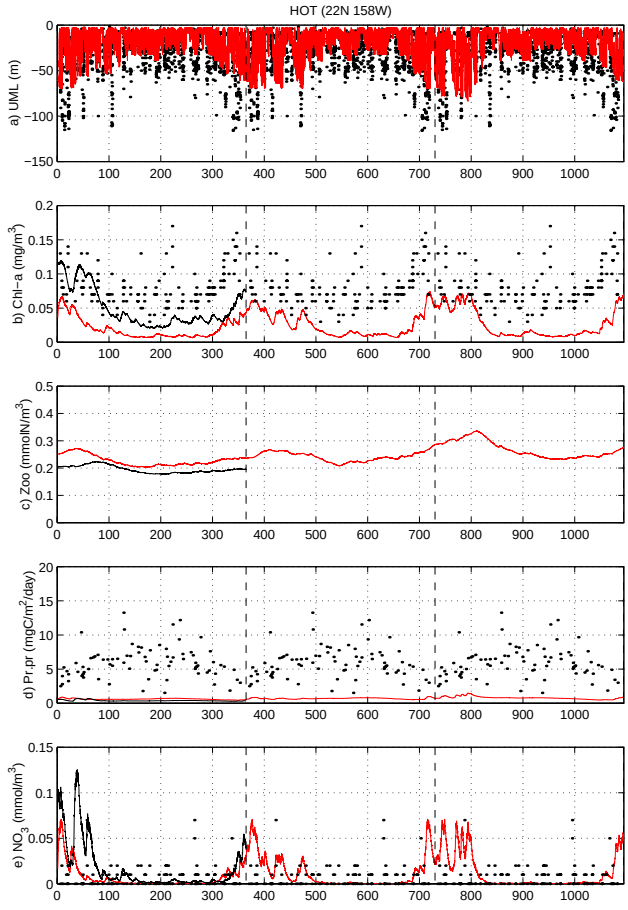

Fig. 3. Annual cycle of modelled (solid line) and observed (dots) ecosystem characteristics at HOT: **(a)** – UML depth (m), **(b)** – surface Chl-a (mg Chl m^{-3}), **(c)** – surface zooplankton biomass (mmol N m^{-3}), **(d)** – UML integrated primary production (mg C m^{-2} d^{-1}), **(e)** – surface nitrate concentration (mmol N m^{-3}). Results of the grazing experiment are shown for the first year as a black line.

for comparison with the model results are from the compilation of Kleypas and Doney (2001) at http://www.dss.ucar.edu/datasets/ds259.0.

3.4.1 Bermuda Atlantic Time-Series Study (BATS), 31° N, 64° W and Hawaii Ocean Time Series (HOT, 22° N, 158° W)

Both BATS and HOT are situated in subtropical gyres and share many ecosystem characteristics. Differences in the exact position of these stations in the gyres determine their fundamental properties. The position of the BATS on the edge of the North Atlantic subtropical gyre gives rise to a much stronger advective influence and deeper UML in winter compared to HOT, resulting in seasonal oligotrophy during summer. Low-nutrient conditions are dominant all year around at the HOT site (Karl et al., 2001), due to its more central, less dynamically active, position in the gyre. The quality of the 3-D model predictions at these stations generally depends on how well the overall features and position of the gyres are described by the physical model. Frequent difficulties encountered when modelling BATS in 3-D circulation models are overestimated values of winter Chl-a and underestimated summer primary production (Fasham et al., 1993; Oschlies et al., 2000).

The main modelled and observed ecosystem characteristics and UML depth for BATS and HOT are compared to observational data in Figs. 2 and 3. According to the observations (Karl et al., 2001), winter-time UML at BATS experiences significant interannual variability and varies between 250 and 500 m. The winter regime at HOT is more stable with UML depth rarely exceeding 120 m. In summer, storm-induced mixing frequently penetrates below 50 m at HOT, while at BATS, which is influenced by large stable high

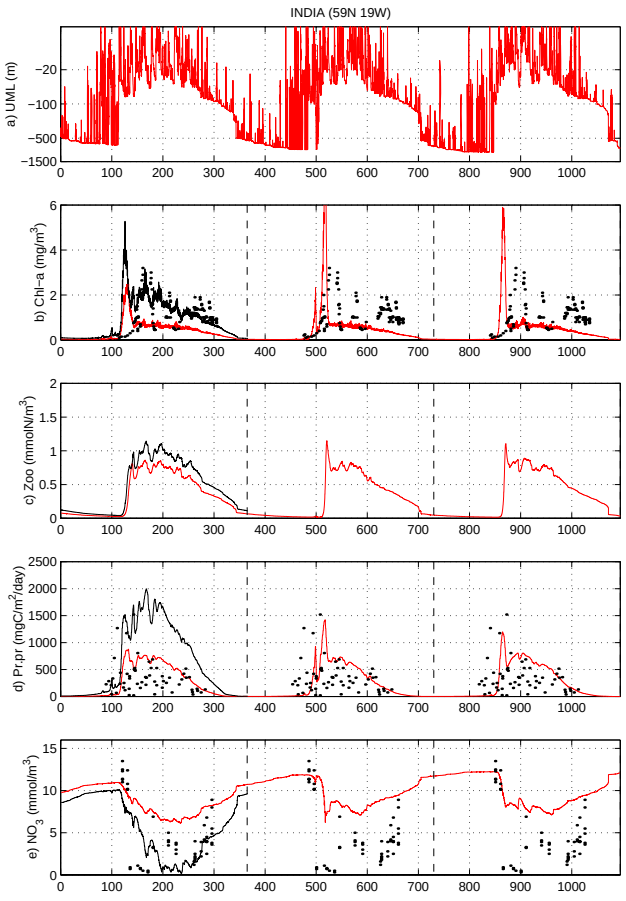

Fig. 4. Annual cycle of modelled (solid line) and observed (dots) ecosystem characteristics at station India: **(a)** – UML depth (m) (note log-scale), **(b)** – surface Chl-a (mg Chl m^{-3}), **(c)** – surface zooplankton biomass (mmol N m^{-3}), **(d)** – UML integrated primary production (mg C m^{-2} d^{-1}), **(e)** – surface nitrate concentration (mmol N m^{-3}). Results of the grazing experiment are shown for the first year as a black line.

pressure systems, it penetrates only to 20–25 m. Modelled UML depth (Figs. 2a, 3a) shows good agreement with these features except that winter mixing in HOT is underestimated. Alternating short periods of storms and stable stratification create pulses of high Chl-a and productivity at both stations, especially in spring.

Model nitrate Figs. 2e, 3e concentrations are in good agreement with observations at both BATS and HOT as well as primary production at BATS (Fig. 2d). At HOT primary production (Fig. 3d) and hence Chl-a (Fig. 3b) are significantly underestimated mostly because of the underestimated mixing. Another possible explanation for this underestimate of the productivity is N_2 fixation (Michaels et al., 2001), which is not represented in the model.

3.4.2 Weather station India (59° N, 19° W), stations Papa (50° N, 145° W), and KERFIX 50° S, 68° E)

Although station India is not one of the JGOFS time series sites, it is an important test for any 3-D model as it is a reasonably well-documented location in an area of deep winter convection. India, Papa and KERFIX are situated approximately at the same latitude in the North Atlantic, North Pacific and Southern Oceans, respectively, but exhibit dramatic differences in the annual cycle of the Chl-a. Modelled and observed UML depth variability and ecosystem characteristics for these stations are shown in Figs. 4 (India), 6 (Papa) and 5 (KERFIX). In the North Atlantic, as is seen in the observations at station India and satellite Chl-a measurements, there is always a pronounced spring bloom of phytoplankton, followed by summer nutrient concentrations that may at times be low enough to limit primary production. In contrast, stations Papa and KERFIX belong to so-called high-nutrient low-chlorophyll (HNLC) areas, where marked phytoplankton blooms do not occur and nutrients remain high all year round. Low Chl-a is observed throughout the year at Station Papa, despite pronounced high primary production during summer. The level of primary production at KERFIX is in contrast much lower. The causes of the production cycle differences between the North Atlantic and North Pacific, and between the North Atlantic and Southern oceans, have been the subject of considerable debate in recent years (e.g. Banse, 1992; Fasham, 1995; Popova et al., 2000). Hypotheses put forward to explain these differences include the effect of light limitation due to the contrasting UML regimes, grazing pressure, and iron availability (Fasham, 1995).

The predicted depth of winter mixing at Station India reaches 600–700 m, with occasional short-term mixing events down to 1200 m during some years (Fig. 4a). At KERFIX the predicted winter mixing penetrates to a depth of 220–260 m (Fig. 5a), in good agreement with observations. At station Papa winter convection as predicted by the model does not penetrate deeper than 130 m, also in good agreement with the observations. Both modelled and observed UML at KERFIX exhibit much deeper mixing in summer (70–100 m) than at the other two stations due to the greater wind stress in the Southern Ocean. Our model results indicate that such a difference in the UML regime is sufficient to explain the difference in the summer productivity. Modelled primary production is in good agreement with observations for all three stations, although in the case of station India it is on the high side of the observed values.

The predicted lack of deep winter convection at KERFIX and Papa, totally unlike India in the North Atlantic at the same latitude (Figs. 4–6a), allows zooplankton in the model to survive throughout the winter months and gives rise to significant grazing pressure on phytoplankton when primary production increases in the spring. At KERFIX predicted zooplankton biomass is about 0.2 mmol N m^{-3} (Fig. 5c) just before the spring restratification in comparison to about

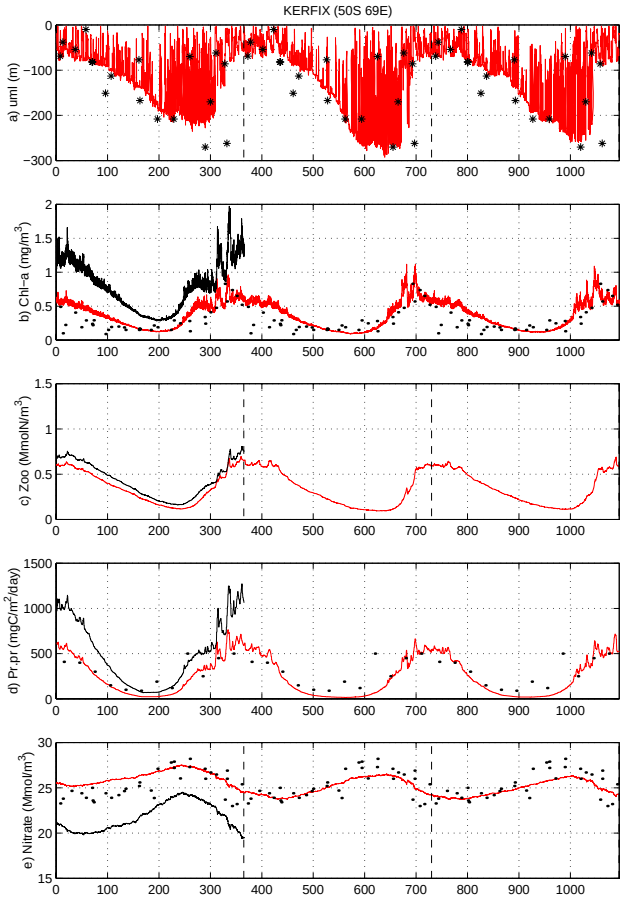

Fig. 5. Annual cycle of modelled (solid line) and observed (dots) ecosystem characteristics at station KERFIX: **(a)** – UML depth (m), **(b)** – surface Chl-a (mg Chl m^{-3}), **(c)** – surface zooplankton biomass (mmol N m^{-3}), **(d)** – UML integrated primary production (mg C m^{-2} d^{-1}), **(e)** – surface nitrate concentration (mmol N m^{-3}). Results of the grazing experiment are shown for the first year as a black line.

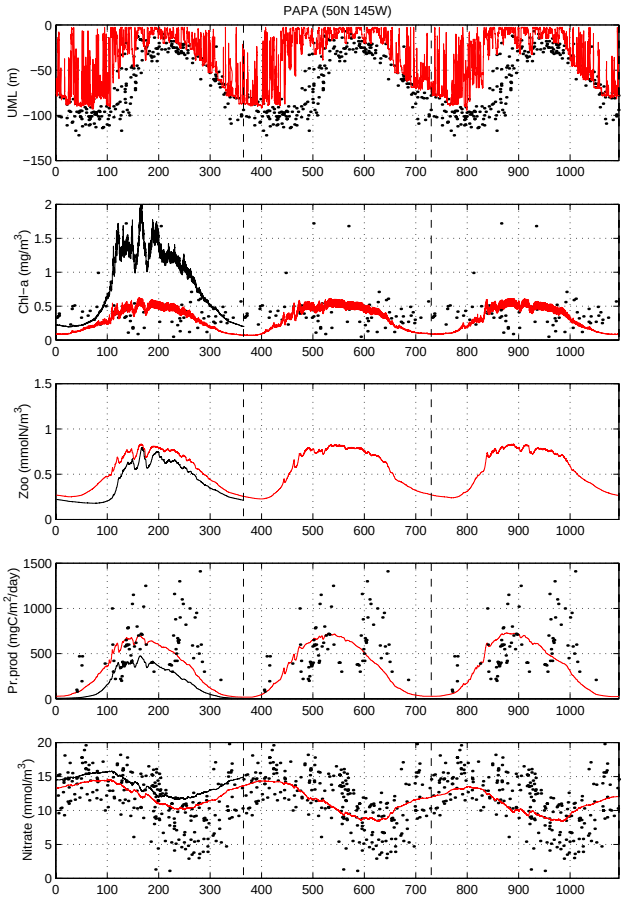

Fig. 6. Annual cycle of modelled (solid line) and observed (dots) ecosystem characteristics at station Papa: **(a)** – UML depth (m), **(b)** – surface Chl-a (mg Chl m^{-3}), **(c)** – surface zooplankton biomass (mmol N m^{-3}), **(d)** – UML integrated primary production (mgC m^{-2} d^{-1}), **(e)** – surface nitrate concentration (mmol N m^{-3}). Results of the grazing experiment are shown for the first year as a black line.

0.3 mmol N m^{-3} at station Papa (Fig. 6c). In contrast modelled zooplankton biomass is practically undetectable at station India prior to the spring bloom (Fig. 4c). As a result the modelled Chl-a bloom at India is very pronounced, reaching values of 5–7 mg Chl m^{-3} (Fig. 4b), with even higher values in years of deeper winter convection. The magnitude of the observed spring bloom is lower, reaching about 3.2 mg Chl m^{-3}. This difference may be associated with grazing control provided by mesozooplankton such as *Calanus*, which undergo diapause in deep water over winter, and then congregate on the surface just before the spring bloom begins (Heath, 1999). Such complex life history strategies are not part of the zooplankton submodel. The modelled phytoplankton bloom is much lower at KERFIX (0.8–1. mg Chl m^{-3}, Fig. 5b), although occurring about a month earlier. It does however correspond closely with the timing of a peak in the recent CZCS derived estimates of primary production of Arrigo et al. (1998) (Fig. 5d) for the Indian sector of the Southern Ocean. At station Papa a spring bloom is absent in both the model and observations (Fig. 6b). The relatively shallow winter UML, and resulting lack of limitation by light, gives rise to high winter values of Chl-a (about 0.2 mg Chl m^{-3}), in good agreement with observations. Strong grazing control maintains low summer values of Chl-a (about 0.5 mg Chl m^{-3}) and high nitrate (with observed minimum values between 3 and 12 mmol N m^{-3} and modelled values at the high end of this range, Fig. 6e) in the model. Such a mechanism for maintenance of the HNLC state in the North Pacific was first suggested by Evans and Parslow (1985).

The major problem encountered by the model at station India, as well as throughout the whole northern North Atlantic, is the late summer regime where observations show significant Chl-a concentrations and even a pronounced

autumn bloom, while model Chl-a remains low (about 0.2 mg Chl m^{-3}) because of strong grazing control. As a consequence of this anomaly, predicted nitrate concentrations in late summer are about double those observed (Fig. 4e). Although observations showing an absence of nutrient depletion during the summer in the northern North Atlantic have been reported not only as far north as station India but also, in some years, for 45° N (Popova et al., 2002), the large spatial extent of high nutrients during late summer in the model (poleward of 30–40° N) is nevertheless an artefact of the model. We can speculate that the reason for this artefact is the lack of mesozooplankton in the model. Introducing it as an additional model state variable with a much lower grazing rate than microzooplankton would provide a switch from high to low grazing control on phytoplankton after the spring bloom. Such a low grazing control will lead to higher phytoplankton biomass, higher primary production and more intense nitrate consumption in the late summer.

4 Role of grazing control at high latitudes

In the analysis of the control run (OB1) we hypothesised that the success of the model in reproducing HNLC conditions is largely determined by the strength of the grazing. On the other hand, problems with the late summer regime in the northern North Atlantic, including underestimated Chl-a and overestimated nitrate, may be a result of modelled grazing being too high in this area. It is possible that in reality late summer in the North Atlantic is dominated by mesozooplankton with a slower growth rate than microzooplankton. In order to examine the significance of grazing pressure on predicted Chl-a further, and discover whether it is possible to find an optimal grazing parameterization to reproduce Chl-a throughout the high latitude oceans, we performed a set of numerical experiments reducing parameter ε (Eqs. B12, B13) until a satisfactory simulation of the nitrate decline at station India in spring was obtained. Reduction by a factor of three gave the desired results, which are shown on Figs. 2–6 as a thick line.

Decreasing parameter ε gave rise to improvement in agreement between modelled and observed nitrate (Fig. 4e). Predicted Chl-a concentration after the spring bloom increased by about factor of two (Fig. 4b), although it still does not show the autumn maximum that is characteristic of the data. This may indicate that an even larger decrease of the grazing rate is needed to improve the general agreement with data at station India. On the other hand, late summer primary production predicted by the model is now about two times higher than is observed (Fig. 4d), although the primary production measurements made in 1971–74 by ^{14}C incubation experiments used outdated methodologies that potentially gave rise to significant errors (e.g. Fitzwater et al., 1982).

Although agreement with data was improved at station India by decreasing parameter ε, the model-data comparisons at the two other high latitude stations KERFIX (Fig. 5) and Papa (Fig. 6) worsened. Predicted primary production and Chl-a at KERFIX were now about two times higher than observed, with the predicted Chl-a during the spring bloom reaching values of about 2 mg Chl m^{-3}. Similarly summer Chl-a predicted at Papa is about 2–3 times higher than in run OB1, now showing a pronounced spring-summer maximum. Primary production is about double that of run OB1, on the high side of observations.

The effect of the reduced grazing on the low latitude stations HOT and BATS is not as dramatic as that predicted at high latitudes. At BATS reduced grazing leads to the lower regeneration of nutrients, which results in lower nitrate and ammonium concentrations and decreased primary production, especially during summer. At HOT, the grazing reduction almost doubled the Chl-a, but did not affect primary production because it is severely limited by nutrients.

5 Discussion

The global coupled biogeochemical model (OB1) with 1° spatial resolution presented here is based on a simple 6 component (Chl-a, P, Z, D, N, A) ecosystem model. Such low complexity in the ecosystem model was deliberately chosen in order to concentrate on examining the effects of physical variability, rather than biological complexity, as the driving force of geographical variations in global ecosystem dynamics. Particular attention was paid to the careful representation of UML depth dynamics in the model. A KPP parameterization of the vertical mixing combined with six-hourly external forcing is employed in OB1. The model successfully reproduces differences in winter convection between the North Atlantic, North Pacific and Southern Oceans, which are largely responsible for the contrasting ecosystem dynamics in these areas. The North Atlantic ecosystem thus exhibits a strong phytoplankton bloom, while blooms in the North Pacific and Southern Ocean are virtually nonexistent because of the strong grazing pressure of overwintering zooplankton. The relatively shallow UML during winter and early spring in these areas permits sufficient phytoplankton production to allow zooplankton to survive, such that grazer biomass is relatively high at the end of this period. Primary production during spring is then matched by zooplankton grazing and a phytoplankton bloom does not occur.

Nevertheless the lack of deep winter convection in the Southern Ocean only partly explains the year round low Chl-a concentrations in this area. There are many areas in the North Atlantic with similar winter UMLs, but which nevertheless exhibit a pronounced phytoplankton bloom. A second factor controlling the low Southern Ocean Chl-a values in the model is severe light limitation of phytoplankton during the summer, due to deep (70–100 m) mixing maintained by high wind stress.

JGOFS time series Papa in the North Pacific, KERFIX in the Southern Ocean and weather station India in the North Atlantic are good examples of the above mentioned ecosystem regimes and present excellent data sets for testing global models against. The simple ecosystem model presented here, in conjunction with an advanced physical model, was able to realistically reproduce these data sets without recourse to introducing a more complex ecosystem model, or different parameterizations for each site except station India. It is interesting that the model has apparently done so well despite the fact that it disregards the effects of iron limitation of phytoplankton growth. Recent simulations of the annual production cycle at KERFIX using a model that does include the role of iron in phytoplankton metabolism (Fasham et al., 2006) have shown that, although growth rate is reduced by iron limitation in summer this effect on primary production is far outweighed by light limitation due to the deep mixed layer. This may explain why our model can give a good representation of the seasonal cycle at KERFIX without taking into account the effect of iron.

The single zooplankton state variable in our model is parameterized to be generally representative of microzooplankton, with a grazing rate that matches phytoplankton growth rate. Decreasing this zooplankton grazing rate in the model led to the disappearance of the all year round low Chl-a regimes at high latitude in the Pacific and Southern Oceans. This result suggests that microzooplankton dominate grazing in the high latitude HNLC systems (e.g. Landry et al., 2002). High nutrient regimes are generally thought to support large phytoplankton (and associated large grazers), small cells being characteristic of oligotrophic conditions (Maranon et al., 2001). In the case of HNLC, however, limitation of primary production by iron may favour smaller phytoplankton, along with their protozoan grazers (e.g. Banse, 1996). However assigning a high grazing rate to zooplankton lessened the agreement between model and data at station India and in general in the northern North Atlantic. Predicted summer Chl-a values were too low and nutrients too high, being quickly restored after the spring bloom by storm events. Mesozooplankton such as *Calanus* may be the dominant grazers in the North Atlantic (Heath, 1999). Grazing by these animals on microzooplankton may suppress their activity and allow phytoplankton to bloom in the autumn, when nutrients are re-entrained into the UML, dynamics which cannot be caputed in the model because it has only a single zooplankton state variable.

An important conclusion following from the model results presented here is therefore that, in spite of the good agreement with data throughout most of the global domain, the model is not globally robust in the sense that additional parameterizations were needed to realistically simulate ecosystem dynamics in the North Atlantic. This conclusion is somewhat unusual for a 3-D global coupled modelling study. Other studies with a similar low complexity biological models have implied the need of alternative parameterizations in the Southern Ocean (Palmer and Totterdell, 2001; Six and Maier-Reimer, 1996).

An important feature of the UML parameterization in the model is its ability to handle short-term episodic events such as storm induced deepening of the UML and short-term winter and spring restratification during the periods of a very calm weather. Such events are not only important in controlling light limitation at high latitudes but are also important source of nutrient supply on the edges of the subtropical gyres (PC06).

Although the emphasis of the work was in keeping the ecosystem model as simple as possible, a novel formulation of zooplankton excretion based on intake rather than biomass was introduced. It is particularly important in ensuring enough nutrient recycling to fuel regenerated production in the oligotrophic gyres. Oschlies et al. (2000) pointed that parameterization of zooplankton excretion as a linear function of biomass results in a threshold phytoplankton biomass below which a zooplankton population cannot be maintained without input via advection or diffusion. In order to overcome this problem zooplankton excretion was made a function of intake rather than biomass, thus assuming that metabolic rate, and associated excretion, are proportional to ingestion rate (Fenchel and Finlay, 1983). Thus excretion rate is low when food is scarce which, in combination with a non-linear zooplankton mortality parameterization, ensures the maintenance of zooplankton populations in the model in the centre of the oligotrophic gyres. A combination of these ecosystem model improvements and an advanced parameterization of UML dynamics capable of reproducing episodic mixing events allowed us to reach good agreement between the main ecosystem characteristics and observations not only at high but also at the low latitudes. It is worth noting that the agreement with data at the centre of the oligotrophic gyres might be further improved by increasing the horizontal resolution of the model which would activate vertical and horizontal eddy-induced nutrient supply to the eupthotic zone.

Whether or not global marine ecosystem dynamics can be realistically simulated using a single robust model with a unique parameter set, and how complicated such a model should be, are important questions confronting today's global biogeochemical modelling community (Anderson, 2005). The work presented here has highlighted the importance of paying attention to the realistic parameterization of physics, particularly of the UML, when undertaking global ocean biogeochemical modelling studies. When confronted with anomalies in model results, the temptation is to blame the simplicity of the ecosystem model, and assume that increasing complexity in this respect will lead to improvement in output. Biological communities throughout the world oceans are certainly diverse, and the use of a typical nutrient-phytoplankton-zooplankton-detritus model structure as here is obviously a considerable compromise. One-dimensional modelling studies using complex ecosystem models have successfully reproduced the biogeochemical dynamics of

JGOFS time-series sites (e.g. Anderson and Pondaven, 2003; Ryabchenko et al., 1997), but it should be noted that these studies also paid considerable attention to ensuring that physics was well represented.

The introduction of new biological parameterizations and additional state variables into 3-D models usually involves significantly less effort than improvement of model physics or its numerical realisation. Moreover biological schemes, carefully parameterized, can target particular areas of the ocean, whereas the parameterization of physics is universal. So, for example, nitrogen fixation might be introduced as a means of increasing nutrient supply to oligotrophic gyres, where primary production is usually grossly underestimated in GCMs. Another means of increasing nutrient supply in these gyres in models is to introduce eddy-induced nutrient pumping, which would require the use of super-high resolution physical models (e.g. McGillicuddy Jr. et al., 2003). This latter approach is certainly more demanding to implement and run. Similarly, simple parameterizations of iron limitation of primary production in the Southern Ocean are relatively easy to put in place, but our work (PC06) has shown that one also needs to consider the importance of high storm frequency when investigating biogeochemical cycling in this region.

A good historical example of the use of a biological "fix" to what was in fact a difficulty of model physics was the "nutrient trapping" problem. Nutrient trapping in models manifested itself as an unrealistic accumulation of nutrients in equatorial areas in the first generation of biogeochemical models (Najjar et al., 1992), shown later to be mainly a numerical artefact (Oschlies, 2000). The controversy was set in motion by the measurement of unrealistically high concentrations of dissolved organic matter as reported by Suzuki et al. (1985) and Sugimura and Suzuki (1988), but later withdrawn (Suzuki, 1993). These high concentrations implied a slow turnover rate which when, albeit unwittingly, incorporated into GCMs permitted equatorial nutrients to dissipate thereby eliminating the nutrient trapping (Bacastow and Maier-Reimer, 1991; Najjar et al., 1992).

Our work here emphasises the need to get the physics, which essentially drives the biogeochemistry, represented realistically in the model first, and then to consider developments in ecosystem modelling. This remark is congruent with the views of A. Oschlies, based on a series of basin-scale modelling studies (Oschlies and Garçon, 1999; Oschlies, 2000, 2001), who called for careful attention to the model physics and numerical realisations before "attempting to correct for a mismatch between model results and observations by adjusting the ecosystem model formulations" (Oschlies, 2000). Of course we are not arguing against the further development of ecosystem models in GCMs. Rather, we are advocating the use of a bottom-up approach in which ecosystem model development is tempered by the need to accurately parameterize physical processes.

This study does not advocate the use of KPP parameterisations as necessarily the best or indeed the most appropriate for the use in global coupled models. It does however show that it is necessary to carefully calibrate the parameterisations used and subsequently analyse results in detail in order to understand the extent to which ecosystem variability is driven by physics, prior to investigation of purely biological factors.

6 Conclusions

(1) A coupled 3-D global model with 1° horizontal resolution is presented, which incorporates a six compartment ecosystem model including Chl-a, phytoplankton, zooplankton, detritus, nitrogen and ammonium. The physical model includes an advanced representation of the UML dynamics based on the KPP parameterization of the upper ocean mixing and six-hourly external forcing. The model realistically reproduces various features of global ecosystem dynamics which have been problematic for previous coupled global models, notably: i) differences in Chl-a and primary production between high latitudes of North Atlantic, North Pacific and Southern Ocean; ii) improved levels of primary and new production in the oligotrophic gyres and equatorial areas.

(2) The model shows improved agreement with observations at the JGOFS time series: BATS, KERFIX, Papa and weather station India as well as with SeaWIFS Chl-a distributions, satellite-derived primary production and the global distribution of nitrate.

(3) The model is able to reproduce the difference in winter convective regimes between the North Atlantic, North Pacific and Southern Ocean. In particular it simulates deep convection in the North Atlantic, and lack of it in the North Pacific and Southern Ocean, as well as deep UMLs in summer in the Southern Ocean due to a high frequency of storm events. When deep winter mixing is absent, phytoplankton biomass in winter stays high enough to support overwintering of microzooplankton, which subsequently graze spring phytoplankton production. In addition, the high frequency external forcing employed in the physical model leads to light limitation in the Southern Ocean in summer, being much more pronounced than in other areas of the ocean.

(4) Primary production in oligotrophic areas is usually seriously underestimated in 3-D coupled models. Our modelled primary production was however in improved agreement with satellite estimates, which we attribute to the high frequency external forcing and careful parameterization of UML depth and zooplankton excretion. Two important sources of nutrient supply to the oligotrophic gyres not included in the model are mesoscale eddy-induced nutrient pumping and nitrogen fixation from the atmosphere.

(5) The model was unable to reproduce the autumn phytoplankton bloom in the North Atlantic because the predicted zooplankton grazing was too high in that area. High grazing was however necessary to reproduce the dynamics of other

areas, notably the HNLC systems. A unique, generic parameter set which characterises the global marine ecosystem was not therefore obtained. Further complexity may need to be introduced to the ecosystem model in future in order to overcome this difficulty.

(6) The work here emphasises the need to get the physics, which essentially drives the biogeochemistry, represented realistically in models first as a prerequisite to developments in ecosystem modelling.

Appendix A

Changes to the K-profile Parametrization (KPP) Model in OCCAM

Here we describe the KPP mixed layer model and the modifications that we made to it. In the KPP model (Large et al., 1997) the boundary layer depth h is diagnosed as the maximum depth at which a bulk Richardson number falls below a specified critical value. In the main text we call this depth "upper mixed layer (UML) depth". Within the boundary layer, the finite diffusivity is set to vary according to an empirically derived profile, tapering off both towards the surface and the thermocline. This boundary layer may be considerably deeper than the well-mixed layer, so allowing vigorous mixing within the thermocline. In convective situations an extra flux is also allowed which may be up the property gradient (the countergradient flux). The KPP model also includes a turbulent contribution towards the bulk Richardson number used to set the depth of the boundary layer. This allows the model to simulate penetrative convection. The model works in three stages.

1. External forcing of tracers and momentum is applied.
2. The boundary layer depth h is diagnosed as the maximum depth at which a bulk Richardson number falls below a specified critical value.
3. Diffusivity and counter gradient flux profiles are calculated, and new depth profiles of momentum and tracers found.

The model assumes that the turbulence near the surface can be described by Monin-Obukhov similarity theory. This theory argues that near the surface, turbulent fluxes vary little with depth and so the only important turbulence parameters are the distance from the boundary and the fluxes through it.

Calculation of diffusivities

Within the boundary layer $-h<z<0$, the vertical turbulent flux of a general quantity X is supposed to take the form

$$\langle wx \rangle = -K_x \left(\frac{\partial X}{\partial z} - \gamma_x \right) \tag{A1}$$

The diffusivity K_x of this quantity X, together with the counter gradient flux $K_x\gamma_x$ must then be determined.

The diffusivity K_x of a property X in the boundary layer is expressed as the product of a depth-dependent velocity scale, $w_x(\sigma)$, and a depth scale made up of the boundary-layer depth h multiplying a non-dimensional shape function $G(\sigma)$:

$$K_x(\sigma) = h w_x(\sigma) G(\sigma). \tag{A2}$$

Here $\sigma=-z/h$ is a dimensionless vertical coordinate that varies from 0 at the surface to 1 at the base of the boundary layer. The shape function $G(\sigma)$ is zero near the surface, together with the length scales of the eddies. It reaches a maximum in the centre of the boundary layer where the eddies are most vigorous, but declines again towards the boundary layer base, $G(\sigma)=1$, as the eddy activity diminishes and the diffusivity falls to thermocline values. In the original model, the shape function is supposed to be a cubic polynomial in σ:

$$G(\sigma) = a_0 + a_1\sigma + a_2\sigma^2 + a_3\sigma^3. \tag{A3}$$

The turbulent velocity scale $w_x(\sigma)$is found by matching to the surface Monin-Obukhov layer. For a neutral boundary layer $w_x(\sigma)=\kappa u_*$, where u_* is the friction velocity $(\tau/\rho_0)^{1/2}$. It is larger when the layer is unstable (convecting) and smaller when the boundary layer is being made more stable by the forcing (warmed).

The vertical profile of $G(\sigma)$ through the boundary layer is plotted in Fig. A1 for the case in which thermocline diffusion is neglected. The values of the a_i are found by matching with the near surface layer and thermocline.

Monin-Obukhov theory implies that $G\to 0$ and $dG/d\sigma\to 1$ near the surface (for appropriate choice of w_x). The other coefficients are obtained by matching the diffusivity and its vertical gradient to the thermocline values at $\sigma=1$. If they can be assumed to be small compared to boundary layer values, which is normally the case given that mixed layer diffusivity $K_x(\sigma)\sim hu_*\sim 10^{-2}m^s s^{-1}$, then $G(1)\sim\left.\frac{dG}{d\sigma}\right|_{\sigma=1}\sim 0$, which leads to the result $G(\sigma)=\sigma(\sigma-1)^2$ shown in Fig. A1.

Calculation of UML depth

The boundary layer thickness, h, is calculated from a constraint on the bulk Richardson number relative to the surface:

$$Ri_b(d) = \frac{(B_r - B(d))\, d}{|\mathbf{v}_r - \mathbf{v}(d)|^2 + \mathbf{v}_t^2(d)}, \tag{A4}$$

and then h is calculated as the largest value of $d=-z$ at which $\mathrm{Ri}_b(d)$ falls below some critical value Ri_c. The standard value of Ri_c is 0.3. Here $B=-g(\rho-\rho_0)/\rho_0$ is buoyancy. The near surface reference velocity, $\mathbf{v_r}$, and buoyancy, B_r, are averages over the near surface layer. The inclusion of the turbulent velocity $\mathbf{v_t}$ in the shear term allows deepening

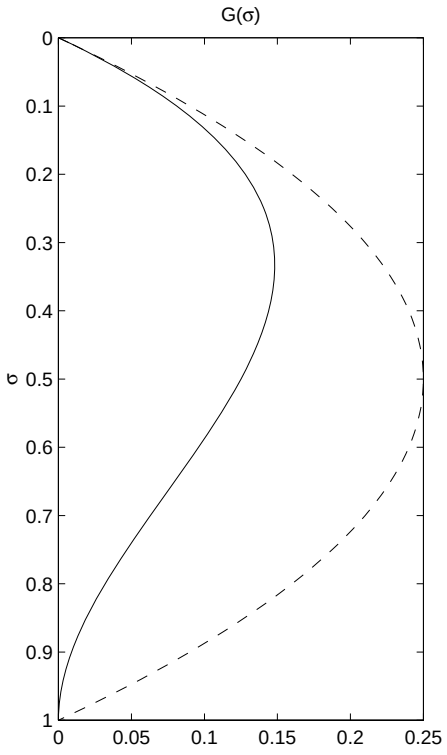

Fig. A1. Vertical profile of the shape function $G(\sigma)$, where $\sigma{=}{-}z/h$, in the special case $G(1){\sim}dG/d\sigma|_{\sigma=1}{\sim}0$. Solid line is the original cubic, dashed line is the simplified quadratic form.

of the boundary-layer even where there is no mean shear, as may occur in pure convection. Hence the model permits penetrative convection.

Problems

We have encountered two major problems with the model as specified above. The first was that the boundary layer was generally too shallow in summer. In many equatorial and subtropical areas this layer was less than 3 m deep, and 20–30 m deep in the ACC in the austral summer, rather than 60–90 m as is to be expected. The second problem was the overestimated depth of winter convection. It was penetrating down to the bottom of the northern North Atlantic and down to 2000–3000 m in the North Pacific and Southern Oceans. These problems led to extreme oligotrophic conditions at low and mid latitudes as well as pronounced spring blooms in the North Pacific and Southern Oceans.

Solution

In order to give deeper summer mixed layers, we use a different G-profile. Following on from Rickard et al. (personal communication)[1], we simply suppose a quadratic profile:

$$G(\sigma) = a_0 + a_1\sigma + a_2\sigma^2. \tag{A5}$$

We use the same boundary conditions at the surface and boundary layer base as before, except that (as the quadratic requires one less boundary condition) we no longer require that $dG/d\sigma$ be continuous at the base of the mixed layer. Since the value $dG/d\sigma$ at the surface is set by Monin-Obukhov theory exactly as before, the quadratic profile gives considerably larger values of diffusivity than did the cubic. For example, assuming again that thermocline diffusivity is negligible in comparison with mixed-layer values, we get $G(\sigma){=}\sigma(1{-}\sigma)$ (the solid line in Fig. A1), which has a maximum of 0.25, in comparison with the cubic (the dashed profile), which has a maximum of ∼0.15. Crucially, the quadratic profile gives larger diffusivities near the base of the mixed layer, where property gradients are stronger, and hence actual fluxes are larger.

This quadratic G-profile gave rise to deeper summer mixed-layer; but also gave winter mixed layers that were far too deep. Depths of 1000–2000 m were attained not only in the North Atlantic but in the North Pacific and Southern Ocean as well. Hence we choose a profile that was a linear combination of the cubic and quadratic profiles, so as to use the quadratic profile for shallow mixed layers and the original cubic profile for deep layers.

The profile is then:

$$G_{\text{comb}}(\sigma) = aG_{\text{cubic}}(\sigma) + (1-a)G_{\text{quadratic}}(\sigma), \tag{A6}$$

where

$$a = 0.5(1 + \tanh[(h - h_0)/D_0]) \tag{A7}$$

with $h_0{=}100$ m and $D_0{=}500$ m.

Results with this formulation seem adequate and are described in the main text in detail.

Appendix B

Biological sources and sinks

The biological variables are phytoplankton P, chlorophyll-a Chl, zooplankton Z, nitrate N, ammonium A, and detritus D. Biological sources and sinks in the photic zone (the top 16 model levels constituting depth of 105 m) are described as follows:

$$B_P = JP(Q_N + Q_A) - G_P - De_P, \tag{B1}$$

$$B_{Chl} = (RJP(Q_N + Q_A) + (-G_P - De_P))\theta\xi^{-1}, \tag{B2}$$

$$B_Z = \delta(\beta_P G_P + \beta_D G_D) - De_Z, \tag{B3}$$

[1]Rickard, G. J., Gordon, C., and Pardaens, A.: personal communication.

$$B_D = (1-\beta_P)G_P - \beta_D G_D - De_D + De_P + \gamma De_Z - w_g \frac{\partial D}{\partial z}, \quad \text{(B4)}$$

$$B_N = -J P Q_N, \quad \text{(B5)}$$

$$B_A = -J P Q_A + De_D + (1-\delta)(\beta_P G_P + \beta_D G_D) + (1-\gamma) De_Z. \quad \text{(B6)}$$

The flux terms (identified in the Notation) are given by

$$R = \frac{\theta_m}{\theta} \frac{J(Q_N + Q_A)}{\alpha I}, \quad \text{(B7)}$$

$$\alpha = \alpha_c \theta \xi^{-1}, \quad \theta = \frac{Chl}{C}, \quad \text{(B8)}$$

$$J = \frac{1}{z_{k+1} - z_k} \int_{z_k}^{z_{k+1}} F(I_0 \exp\{-(k_w + k_c P)z\}) dz, \quad \text{(B9)}$$

$$F(I) = \frac{V_p \alpha I}{(V_p^2 + \alpha^2 I^2)^{1/2}}, \quad \text{(B10)}$$

$$Q_N = \frac{N \exp(-\Psi A)}{k_N + N}, \quad Q_A = \frac{A}{k_A + A}, \quad \text{(B11)}$$

$$G_P = \frac{g \varepsilon p_P P^2 Z}{g + \varepsilon(p_P P^2 + p_D D^2)}, \quad \text{(B12)}$$

$$G_D = \frac{g \varepsilon p_D D^2 Z}{g + \varepsilon(p_P P^2 + p_D D^2)}, \quad \text{(B13)}$$

$$De_P = \frac{\mu_P P^2}{P + k_p}, \quad De_Z = \frac{\mu_Z Z^3}{Z + k_z}, \quad De_D = \mu_D D. \quad \text{(B14)}$$

Biological sources and sinks below the photic zone are described as follows:

$$B_P = -\lambda_{\text{bio}} P, \quad \text{(B15)}$$

$$B_{Chl} = -\lambda_{\text{bio}} Chl, \quad \text{(B16)}$$

$$B_Z = -\lambda_{\text{bio}} Z, \quad \text{(B17)}$$

$$B_D = \lambda_{\text{bio}}(P + Z) - \mu_D D - w_g \frac{\partial D}{\partial z}, \quad \text{(B18)}$$

$$B_A = -\lambda_A A, \quad \text{(B19)}$$

$$B_N = \lambda_A A + \mu_D D. \quad \text{(B20)}$$

Table B1. Notation.

A	concentration of the ammonium (mmol N m^{-3}), model state variable
α	initial slope of $P-I$ curve, (W m^{-2})$^{-1}$ day^{-1}.
α_c	Chl-a specific initial slope of $P-I$ curve, equal to 0.02 gC g Chl^{-1} (W m^{-2})$^{-1}$ day^{-1}.
β_P, β_D	assimilation coefficients of zooplankton, equal to 0.75, 0.75
B_A	ammonium biological sources and sinks (mmol N m^{-3} d-1)
B_P	phytoplankton biological sources and sinks (mmol N m^{-3} d-1)
B_{Chl}	Chlorophyll-a biological sources and sinks (mg C m^{-3} d-1)
B_D	detritus biological sources and sinks (mmol N m^{-3} d-1)
B_N	nitrate biological sources and sinks (mmol N m^{-3} d-1)
B_Z	zooplankton biological sources and sinks (mmol N m^{-3} d-1)
Chl	concentration of the chlorophyll-a (mg C m^{-3})), model state variable
D	concentration of the detritus (mmol N m^{-3}), model state variable
De_D	rate of breakdown of detritus to ammonium
De_P	rate of phytoplankton natural mortality
De_Z	rate of zooplankton natural mortality
ε	grazing parameter relating the rate of capture of prey items to prey density equal to 3.3
δ	excretion parameter
G_P, G_D	grazing rates of the zooplankton on the phytoplankton and detritus
g	zooplankton maximum growth rate equal to 1.3 d^{-1}
γ	fraction of zooplankton mortality going to detritus
I_0	photosynthetically active radiation (PAR) immediately below the surface of the water (assumed to be proportional to the absorbed total solar radiation at the sea surface with the coefficient 0.4)
J	light-limited phytoplankton growth rate (d^{-1})
k_A	half-saturation constant for ammonium uptake, equal to 0.5 mmol m^{-3}
k_N	half-saturation constant for nitrate uptake, equal to 0.5 mmol m^{-3}
k_w	light attenuation due to water, equal to 0.04 m^{-1}
k_c	phytoplankton self-shading coefficient equal to 0.03 m^2 mmol^{-1}
λ_{bio}	rate of the phytoplankton and zooplankton transfer into detritus below the photic zone, equal to 0.1 day^{-1}
λ_A	nitrification rate below the photic zone, equal to 0.03 day^{-1}
N	concentration of the nitrate (mmol m^{-3}), model state variable
μ_P	phytoplankton mortality rate, equal to 0.05 d^{-1}
μ_Z	zooplankton mortality rate, equal to 0.2 d^{-1}(mmolm^3)$^{-3}$
μ_D	detritus reference remineralisation rate, equal to 0.05 d^{-1}
Ψ	strength of ammonium inhibition of nitrate uptake equal to 2.9 (mmolm^{-3})$^{-1}$
P	phytoplankton biomass (mmol N m^{-3}), model state variable
p_P	relative grazing preference for phytoplankton, equal to 0.75
p_D	relative grazing preference for detritus, equal to 0.25
Q_N	non-dimensional nitrate limiting factor
Q_A	non-dimensional ammonium limiting factor
R	ratio of Chl synthesis to carbon fixation
T	temperature (model state variable)
V_p	maximum growth rate of phytoplankton equal 1 day^{-1}
w_g	detritus sinking velocity, equal to 10 md^{-1}
Z	zooplankton biomass (mmol N m^{-3}), model state variable
z	depth
z_i	depth of the model levels.
θ	Chl to carbon ratio, mg Chl mgC^{-1}
θ_m	maximum Chl to C ratio, equal to 0.05 mg Chl mgC^{-1}
ξ	conversion factor from gC to mmolN based on C:N ratio of 6.5, equal to 12.8 mmolN mgC^{-1}

Acknowledgements. The work had been supported by the Natural Environment Research Council core strategic programs BICEP (Biophysical Interactions and Controls on Export Production) and LSTOC (Large Scale Long Term Ocean Circulation).

Edited by: V. Garcon

References

Aksenov, Y.: The sea ice-ocean global coupled model, ARCICE Project Report Part 1: Description of the Dynamical-Thermodynamical Sea Ice Model, Southampton Oceanography Centre, Southampton, UK, 2002.

Anderson, T. R. and Pondaven, P.: Non-redfield carbon and nitrogen cycling in the Sargasso Sea: pelagic imbalances and export flux, Deep-Sea Res. I, 50, 573–591, 2003.

Anderson, T. R.: Plankton functional type modelling: running before we can walk?, J. plankton research, 27, 1073–1081, 2005.

Antoine, D., Andre, J.-M., and Morel, A.: Oceanic primary production, 2, Estimation at global scale from satellite (coastal zone color scanner) chlorophyll, Global Biogeochem. Cy., 10, 57–69, 1996.

Arakawa, A.: Computational design for long-term numerical integration of the equations of fluid motion: Two-dimentional incompressible flow, Part 1., J. Comput. Phys., 1, 119–143, 1966.

Arrigo, K. R., Worthen, D., Schnell, A., and Lizotte, M. P.: Primary production in Southern Ocean waters, J. Geophys. Res., 103, 15 587–15 600, 1998.

Aumont, O., Maier-Reimer, E., Blain, S., and Monfray, P.: An ecosystem model of the global ocean including Fe, Si, P colimitations, Global Biogeochem. Cy., 17, 29.1–29.15, doi:10.1029/2001GB001745, 2003.

Bacastow, R. and Maier-Reimer, E.: Dissolved organic carbon in modelling oceanic new production, Global Biogeochem. Cy., 5, 71–85, 1991.

Banse, K.: Grazing, temporal changes of phytoplankton concentrations, and the microbial loop in the open sea, in: Primary productivity and biogeochemical cycles in the sea, edited by: Falkowski, P. G. and Woodhead, A. D., Plenum Press, New York, pp. 409–440, 1992.

Banse, K.: Low seasonality of low concentration of surface chlorophyll in the Subantarctic water ring: Underwater irradiance, iron or grazing?, Prog. Oceanogr., 37, 241–291, 1996.

Behrenfeld, M. J. and Falkowski, P. G.: A consumers guide to phytoplankton primary productivity models, Limnol. Oceanogr., 42, 1479–1491, 1997.

Berger, W. F., Fischer, K., Lai, C., and Wu, G.: Oceanic productivity and organic carbon flux. Part 1, overview and maps of primary production and and export production, Scripps Institution of Oceanography, SIO Reference 87–30, pp. 1–67, 1987.

Bishop, J. K. B. and Rossow, W. B.: Spatial and temporal variability of global surface solar irradiance, J. Geophys. Res., 96, 16 839–16 858, 1991.

Bissett, W. P., Walsh, J. J., Dieterle, D. A., and Carder, K. L.: Carbon cycling in the upper waters of the Sargasso Sea: I. Numerical simulation of differential carbon and nitrogen fluxes, Deep-Sea Res. I, 46, 205–269, 1999.

Blanke, B. and Delecluse, P.: Low frequency variability of the tropical Atlantic ocean simulated by a general circulation model with mixed layer physics, J. Phys. Oceanogr., 23, 1038–1053, 1993.

Bopp, L., Monfray, P., Aumont., O., Dufresne, J.-L., Treut, H. L., Madec, G., Terray, L., and Orr, J. C.: Potential impact of climate change on marine export production, Global Biogeochem. Cy., 15, 81–99, 2001.

Bryan, K.: A numerical method for the study of the circulation of the world ocean, J. Comput. Phys., 4, 347–376, 1969.

Campbell, J., Antoine, D., Armstrong, R., et al.: Comparison of algorithms for estimating ocean primary production from surface chlorophyll, temperature and irradiance, Global Biogeochem. Cy., 16, 9.1–9.15, doi:10.1029/2001GB001444, 2002.

Cloern, J. E., Grenz, C., and Vidergar-Lucas, L.: An impirical model of phytoplankton Chlorophyll: Carbon ratio – the conversion factor between productivity and growth rate, Limnol. and Oceanogr., 40, 1313–1321, 1995.

Conkright, M. E., Garcia, H. E., O'Brian, T. D., Locarnini, R. A., Boyer, T. P., Stephens, C., Antonov, J. I., and Levitus, S.: World Ocean Atlas Nutrients, NOAA Atlas NESDIS No. 52(4), 392pp, 2001.

Cox, M. D.: A primitive equation three-dimensional model of the ocean. GFDL Ocean Group Tech. Rep. 1, Geophysical Fluid Dynamics Laboratory/NOAA, Princeton University, NJ, 143pp, 1984. (Available from GFDL/NOAA, Princeton University, Princeton, NJ 08542.)

Coward, A. C., Kilworth, P. D., and Blundell J. R.: Test of a two-grid world ocean model, J. Geophys. Res., 99, 22 725–22 735, 1994.

Doney, S. C.: Major challenges confronting marine biogeochemical modelling, Global Biogeochem. Cy., 13, 705–714, 1999.

Ducklow, H. W.: Biogeochemical provinces: towards a JGOFS synthesis, in: Ocean biogeochemistry: the role of the ocean carbon cycle in global change, edited by: Fasham, M. J. R., 99–121, Springer-Verlag Berlin, 2003.

Epply, R. W. and Peterson, B. J.: Particulate organic matter flux and planktonic new production in the deep ocean, Nature, 282, 677–680, 1979.

Evans, G. T. and Parslow, J. S.: A model of annual plankton cycles, Biological Oceanogr., 3, 327–347, 1985.

Falkowski, P. G., Laws, E. A., Barber, R. T., and Murray, J. W.: Phytoplankton and their role in primary, new and export production, in: Ocean biogeochemistry: the role of the ocean carbon cycle in global change, edited by: Fasham, M. J. R., 99–121, Springer-Verlag Berlin, 2003.

Fasham, M. J. R. and Evans, G. T.: The use of optimisation techniques to model marine ecosystem dynamics at the JGOFS station at 47° N 20° W, Phil. Trans. Roy. Soc. Lond., B 348, 206–209, 1995.

Fasham, M. J. R., Ducklow, H. W., and McKelvie, S. M.: A nitrogen-based model of plankton dynamics in the oceanic mixed layer, J. Mar. Res., 48, 591–639, 1990.

Fasham, M. J. R.: Variations in the seasonal cycle of biological production in subarctic oceans: A model sensitivity analysis, Deep Sea Res., 42, 1111–1149, 1995.

Fasham, M. J. R., Sarmiento, J. L., Slater, R. D., Ducklow, H. W., and Williams, R.: Ecosystem behaviour at Bermuda station "S" and Ocean Weather Station India: A general circulation model and observational analysis, Global Biogeochem. Cy., 7, 379–415, 1993.

Fasham, M. J. R., Flynn, K. J., Pondaven, P., Anderson T. R., and

Boyd, P. W.: Development of a robust marine ecosystem model to predict the role of iron in biogeochemical cycles: A comparison of results for iron-replete and iron-limited areas, and the SOIREE iron-enrichment experiment, Deep-Sea Research I, 53, 333–366, 2006.

Fenchel, T. and Finlay, B. J.: Respiration rates in heterotrophic, free-living protozoa, Microb. Ecol., 9, 99–122, 1983.

Fitzwater, S. E., Knauer, G., and Martin, J. H.: Metal contamination and its effect on primary production measurements, Limnol. Oceanogr., 27, 544–551, 1982.

Follows, M. and Dutkiewicz, S.: Meteorological modulation of the North Atlantic spring bloom, Deep-Sea Res. I, 49, 321–344, 2002.

Frost, B. W.: The role of grazing in nutrient-rich areas of the open sea, Limnol. and Oceanogr., 36, 1616–1630, 1991.

Gaspar, P., Gregoris, Y., and Lefevre, J.-M.: A simple eddy kinetic energy model for simulations of the oceanic vertical mixing: Test at station Papa and Long-Term Upper Ocean Study site, J. Geophys. Res., 95, 16 179–16 193, 1990.

Gloersen, P. and Campbell, W. J. : Variations in the Arctic, Antarctic, and global sea ice cover during 1978–1987 as observed with Nimbus-7 SMMR, J. Geophys. Res., 93, 10 666–10 740, 1998.

Gregg, W. W., Conkright, M. E., Ginoux, P., O'Reilly, J. E., and Casey, N. W.: Ocean primary production and climate: global decadal changes, Geophys. Res. Lett., 30, 3.1.–3.4, doi:10.1029/2003GL016889, 2003.

Griffies, S. M.: The Gent-McWilliams skew flux, JPO, 28(5), 831–841, 1998.

Heath, M. R.: The ascent migration of Calanus finmarchicus from overwintering depths in the Faroe-Shetland Channel, Fish. Oceanogr., 8 (Suppl. 1), 84–99, 1999.

Hood, R. R., Bates, N. R., Capone, D. G., and Olson, D. B.: Modeling the effect of nitrogen fixation on carbon and nitrogen fluxes at BATS, Deep-Sea Res. II 48, 1609–1648, 2001.

Hunke, E. C. and Dukowicz, J. K.: An elastic-viscous-plastic model for sea ice dynamics, J. Phys. Oceanogr., 27(9), 1849–1867, 1997.

Jenkins, W. J.: Oxygen utilisation rates in north Atlantic subtropical gyre and primary production in oligotrophic systems, Nature, 300, 246–248, 1982.

Kalnay, E., Kanamitsu, M., Kistler, R., Collins, W., Deaven, D., Gandin, L., Iredell, M., Saha, S., White, G., Woollen, J., Zhu, Y., Chelliah, M., Ebisuzaki, W., Higgins, W., Janowiak, J., Mo, K., Ropelewski, C. C., Leetmaa, A., Reynolds, R., and Jenne, R.: The NCEP/NCAR 40 years reanalysis project, Bull. Amer. Meteorol. Soc., 77(3), 437–506, 1996.

Kara, A. B., Rochford, P. A., and Hurlburt, H. E.: An optimal definition for ocean mixed layer depth, J. Gephys. Res., 105, 16 803–16 821, 2000a.

Kara, A. B., Rochford, P. A., and Hurlburt, H. E.: Mixed layer depth variability and barrier layer formation over the North Pacific Ocean, J. Geophys. Res., 105, 16 783–16 801, 2000b.

Kara, A. B., Rochford, P. A., and Hurlburt, H. E.: Mixed layer depth variability over the global domain, J. Geophys. Res., 108, 24.1–24.15, doi:10.1029/2000JC000736, 2003.

Karl, D. M., Christian, J. R., Dore, J. E., Hebel, D. V., Letelier, R. M., Tupas, L. M., and Winn C. D.: Seasonal and interannual variability in primary production and particle flux at Station ALOHA, Deep-Sea Res. II, 43, 539–568, 1996.

Karl, D. M., Dore, D. E., Lucas, R., Michaels, A. F., Bates, N. R., and Knap, A.: Building the long-term picture: the US JGOFS time-series Programs, Oceanogr., 14, 6–17, 2001.

Kleypas, J. A. and Doney, S. C.: Nutrients, chlorophyll, primary production and related biogeochemical properties in the ocean mixed layer. A compilation of data collected at nine JGOFS sites, NCAR Technical Note NCAR/TN-447+STR, 55pp, 2001.

Landry, M. R., Selph, K. E., Brown, S. L., Abbott, M. R., Measures, C. I., Vink, S., Allen, C. B., Calbet, A., Christensen, S., and Nolla, H.: Seasonal dynamics of phytoplankton in the Antarctic Polar Front region at 170W, Deep Sea Res. II, 49, 1843–1865, 2002.

Large, W. G., Danabasoglu, G., and Doney, S. C.: Sensitivity to Surface Forcing and Boundary Layer Mixing in a Global Ocean Model: Annual-Mean Climatology, J. Phys. Oceanogr., 27, 2418–2446, 1997.

Laws, E. A., Falkowski, P. G., Smith Jr., W. O., Ducklow, H., and McCarthy, J. J: Temperature effects on export production in the open ocean, Global Biogeochem. Cy., 14, 1231–1246, 1982.

Levitus, S.: Climatological Atlas of the World Ocean, 1982, NOAA Prof. Paper, 13, GFDL, Princeton Univ., N. J., 173pp, 2000.

Levitus, S. and Boyer, T.: World Ocean Atlas, Volume 4 Temperature, NOAA Atlas NESDIS 4, 117pp, 1994.

Levitus, S., Burgett, R., and Boyer, T.: World Ocean Atlas, Volume 3, Salinity, NOAA Atlas NESDIS 3, 99pp, 1994.

Longhurst, A.: Seasonal cycles of pelagic production and consumption, Prog. Oceanogr., 36, 77–167, 1995.

Lumpkin, R. and Flament, P.: Lagrangian statistics in the central North Pacific J. Mar. Syst. 29, 141–155, 2001.

Maier-Reimer, E., Mikolajewicz, U., and Hasselmann, K.: Mean circulation of the Hamburg LSG OGCM and its sensitivity to the thermohaline surface forcing, J. Phys. Oceanogr., 23, 731–757, 1993.

Maranon, E., Holligan, P. M., Varela, M., Mourino, B., and Bale, A. J.: Basin-scale variability of phytoplankton biomass, production and growth in the Atlantic Ocean, Deep-Sea Research I, 47, 825–857, 2000.

Maranon, E., Holligan, P. M., Barciela, R., Gonzalez, N., Mourino, B., Pazo, M., and Varela, M.: Patterns of phytoplankton size structure and productivity in contrasting open-ocean environments, Mar. Ecol. Prog. Ser., 216, 43–56, 2001.

Martin, J. H.: Glacial-interglacial change: The iron hypothesis, Paleoceanography, 5, 1–13, 1990.

Mellor, G. L. and Yamada, T.: A hierarchy of turbulent closure models for planetary boundary layers, J. Atmos. Sci., 31, 1791–1806, 1974.

Michaels, A. F., Karl, D. M., and Capone, D. G.: Element stoichiometry, new production and nitrogen fixation, Oceanogr., 14, 68–77, 2001.

McGillicuddy Jr., D. J., Robinson, A. R., Siegel, D. A., Jannasch, H. W., Johnson, R., Dickey, T. D., McNeil, J., Michaels, A. F., and Knap, A. H.: Influence of mesoscale eddies on new production in the Sargasso Sea, Nature, 394, 263–265, 1998.

McGillicuddy, D. J. Jr., Anderson, L. A. , Doney, S. C., and Maltrud, M. E.: Eddy-driven sources and sinks of nutrients in the upper ocean: Results from a 0.1° resolution of the North Atlantic, Global Biogeochem. Cy., 17, 4.1–4.20, doi:10.1029/2002GB001987, 2003.

Moore, J. K., Doney, S. C., Kleypas, J. A., Glover, D. M., and Fung,

I. Y.: An intermediate complexity marine ecosystem model for the global domain, Deep-Sea Research II, 49, 403–462, 2002.

Najjar, R. G., Sarmiento, J. L., and Toggweiler, J. R.: Downward transport and fate of organic matter in the oceans: simulations with a general circulation model, Global Biogeochem. Cy., 6, 45–76, 1992.

Oschlies, A.: Equatorial nutrient trapping in biogeochemical ocean models: the role of advection numerics, Global Biogeochem. Cy., 14, 655–667, 2000.

Oschlies, A.: Model-derived estimates of new production: New results point towards lower values, Deep-Sea Research II, 48, 2173–2197, 2001.

Oschlies, A. and Garçon, V.: An eddy-permitting coupled physical-biological model of the North Atlantic 1. Sensitivity to advection numerics and mixed layer physics, Global Biogeochem. Cy., 13, 135–160, 1999.

Oschlies, A., Koeve, W., and Garçon, V. : An eddy-permitting coupled physical-biological model of the North Atlantic 2. Ecosystem dynamics and comparison with satellite and JGOFS local studies data, Global Biogeochem. Cy., 14, 499–523, 2000.

Pacanowski, R. C.: MOM 2 documentation, user's guide and reference manual. GFDL Ocean Group Tech. Rep. 3, Geophysical Fluid Dynamics Laboratory/NOAA, Princeton University, NJ, 232pp, 1995. (Available from GFDL/NOAA, Princeton University, Princeton, NJ 08542.).

Palmer, J. R. and Totterdell, I. J.: Production and export in a global ecosystem model, Deep-Sea Research I, 48, 1169–1198, 2001.

Paulson, C. A. and Simpson, J. J.: Irradiance measurements in the upper ocean, J. Phys. Oceanogr., 7, 952–956, 1977.

Pondaven, P., Ruiz-Pino, D., Fravalo, C., Treguer, P., and Jeandel, C.: Interannual variability of Si and N cycles at the time-series station KERFIX between 1990 and 1995 – a 1-D modelling study, Deep-Sea Research I, 47(2), 223–257, 2000.

Popova, E. E., Lozano, C. J., Srokosz, M. A., Fasham, M. J. R., Haley, P. J., and Robinson, A. R.: Coupled 3-D physical and biological modeling of the mesoscale variability in northeast Atlantic in spring 1997: biological processes, Deep Sea Research I, 49, 1741–1768, 2002.

Popova, E. E., Ryabchenko, V. A., and Fasham, M. J. R.: Biological pump and vertical mixing in the Southern Ocean: their impact on atmospheric pCO2, Global Biogeochem. Cy., 14(1), 477–498, 2000.

Popova, E. E., Coward, A. C., Nurser, G., De Cuevas, B., and Anderson, T. R.: Mechanisms controlling primary and new production in a global ecosystem model. Part II: The role of the short-term upper ocean periodic and episodic mixing events, Ocean Sci., 2, 267–279, 2006, http://www.ocean-sci.net/2/267/2006/.

Roemmich, D., Morris, M. Y., Young, W. R., and Donguy, J. R.: Fresh equatorial jets, J. Phys. Oceanogr., 24, 540–558, 1994.

Rossow, W. B. and Schiffer, R. A.: ISCCP Cloud Data Products, Bull. Amer. Meteor. Soc., 72, 2–20, 1991.

Ryabchenko, V. A., Fasham, M. J. R., Kagan, B. A., and Popova E. E.: What causes short-term oscillations in ecosystem models of the ocean mixed layer?, J. Mar. Systems, 13, 33–50, 1997.

Sarmiento, J. L., Slater, R. D., Fasham, M. J. R., Ducklow, H. W., Toggweiler, J. R. and Evans, G. T.: A seasonal three-dimensional ecosystem model of nitrogen cycling in the North Atlantic euphotic zone, Global Biogeochem. Cy., 7, 417–450, 1993.

Saunders, P. M., Coward, A. C., and de Cuevas, B. A.: The Circulation of the Pacific Ocean seen in a Global Ocean Model (OCCAM), J. Geophys. Res., 104, C8, 18 281–18 299, 1999.

Semtner, A. J.: A general circulation model for the World Ocean, Tech. Rep, 9, Department of meteorology, University of California, Los Angeles, CA, 99pp, 1974.

Six, K. D. and Maier-Reimer, E.: Effects of plankton dynamics on seasonal carbon fluxes in an ocean general circulation model, Global Biogeochem. Cy., 10, 559–583, 1996.

Spencer, R. W.: Global oceanic precipitation from the MSU during 1979–91 and comparisons to other climatologies, J. Climate, 6, 1301–1326, 1993.

Sugimura, Y. and Suzuki, Y.: A high-temperature catalytic oxidation method for the determination of non-volatile dissolved organic carbon in seawater by direct injection of a liquid sample, Mar. Chem., 24, 105–131, 1988.

Sundquist, E. T.: Geological perspectives on carbon dioxide and the carbon cycle, Geophysical Monographs, 32, 5–59, 1985.

Suzuki, Y.: On the measurement of DOC and DON in seawater, Mar. Chem., 41, 287–288, 1993.

Suzuki, Y., Sugimura, Y., and Itoh, T.: A catalytic oxidation method for the determination of total nitrogen dissolved in seawater, Mar. Chem., 16, 83–97, 1985.

Sverdrup, H. U.: On the conditions for the vernal blooming of phytoplankton, J. Cons. Perm. Int. Explor. Mer., 18, 287–295, 1953.

Taylor, A. H., Geider, R. J., and Gilbert, F. J. H.: Seasonal and latitudinal dependencies of phytoplankton carbon-to-chlorophyll a ratios: results of a modelling study, Mar. Ecol. Prog. Ser., 152, 51–66, 1997.

Webb, D. J., de Cuevas, B. A., and Richmond, C. S.: Improved advection schemes for ocean models, J. Atmos. Ocean. Tech., 15, 1171–1187, 1998.

Williams, R. G. and Follows, M. J.: Physical transport of nutrients and maintenance of biological production, in: Ocean biogeochemistry: the role of the ocean carbon cycle in global change, edited by: Fasham, M. J. R., Springer-Verlag Berlin, 19–52, 2003.

Xie, P. and Arkin, P. A.: Global precipitation: a 17-year monthly analysis based on gauge observations, satellite estimates, and numerical model outputs, Bullet of the American Meteorological Society, 78(11), 2539–2558, 1997.